ELSEVIER

Journal of Power Sources 113 (2003) 101–108

JOURNAL OF POWER SOURCES

www.elsevier.com/locate/jpowsour

In-plane gradients in fuel cell structure and conditions for higher performance☆

David P. Wilkinson, Jean St-Pierre*

Ballard Power Systems, 9000 Glenlyon Parkway, Burnaby, BC, Canada V5J 5J9

Received in revised form 26 August 2002; accepted 10 September 2002

Abstract

A major challenge to full commercialization of the polymer electrolyte fuel cell (PEFC) is the cost of materials and performance. A focus for research and development is to reduce material costs while maintaining or improving performance under practical operating conditions. The challenge to reach optimal performance in commercial fuel cells requires optimization of electrochemical activity over the entire active area. This is necessary because in a practical fuel cell as reactants pass along the flow field channels between inlet and outlet the composition and other parameters will change as the reactant is consumed and products are formed.

Keywords: Polymer electrolyte fuel cell; Cell performance; In-plane gradients; Cell design

1. Introduction

In the past, polymer electrolyte fuel cell (PEFC) technology has mainly been concerned with providing uniform conditions and structures over the active area. The conventional approach to operating conditions has been to provide more uniform conditions through higher reactant stoichiometries and isothermal conditions. There has been more focus on controlling transport phenomena and conditions in the "z" direction (perpendicular to the electrode plane) but not in the electrode plane [1]. At any point across the active area between the inlet and outlet the structure and composition of the electrode was kept essentially constant.

The absence of strategies to enhance cell performance by introducing cell non-uniformities in the electrode plane is surprising, considering that a substantial number of studies were dedicated to the understanding of the changes occurring along the gas flow fields within PEFCs. There are a few models available discussing cell performance, water management and heat management issues as a function of the position along the flow field [2–10]. Methods to determine current distribution [11–13] and potential distribution [14] have also been published. Recently, a process aimed at the production of graded porous materials was also discussed [15], which may provide some interesting possibilities for fuel cell gas diffusion electrode design.

In this paper, the advantages of providing non-uniformity and gradients in the fuel cell will be discussed. In particular, methods of varying the electrochemical activity characteristics in and across the plane of the electrode to accommodate variations in gas concentration and flow, water flux and temperature variation will be discussed. Diagnostic techniques and analytical tools previously developed [13] have been applied to determine optimal structures and gradients. These approaches can enhance both the electrochemical performance obtained from the fuel cell and enhance the efficient use of platinum group metals and other costly materials.

2. Experimental

Standard Ballard Mk5 and Mk513 fuel cells were used. Whereas the Mk5 fuel cell was operated isothermally to the extent possible, the Mk513 fuel cell was operated with a temperature gradient between the inlet and outlet coolant ports. Standard Ballard test equipment (external humidifier, gas mixer, test station and electronic load) that controls gas type and composition, flows, pressures, relative humidities, temperature and cell current density were also used. Commercial multimeters, milliohmmeters, pressure gauges and

☆ Presented at the 195th Meeting of The Electrochemical Society, 2–6 May 1999.

* Corresponding author. Tel.: +1-604-412-3186; fax: +1-604-453-3782.
E-mail address: jean.st-pierre@ballard.com (J. St-Pierre).

0378-7753/02/$ – see front matter
PII: S0378-7753(02)00486-X

Nomenclature

A	geometric electrode area
c_O	oxygen concentration in the oxidant stream
C_p	water heat capacity
F	Faraday constant
i	average current density
N_g	air molar flow rate
N_H	hydrogen molar flow rate
$N_{H,0}$	fuel inlet hydrogen molar flow rate
N_O	oxygen molar flow rate
N_v	water vapor molar flow rate
$N_{v,0}$	fuel inlet water vapor molar flow rate (co-flow)
$N_{v,1}$	fuel inlet water vapor molar flow rate (counter-flow)
p	gas pressure
p_s	water vapor saturation pressure
$p_{s,0}$	fuel inlet water vapor saturation pressure (co-flow)
$p_{s,1}$	fuel inlet water vapor saturation pressure (counter-flow)
p_v	water vapor partial pressure
R	membrane resistance
RH	relative humidity
RH_0	fuel inlet relative humidity (co-flow)
RH_1	fuel inlet relative humidity (counter-flow)
T	temperature
T_0	coolant inlet temperature
V	cell voltage
V_{tn}	thermoneutral voltage
$\dot{V}$	volumetric coolant flow rate
X	dimensionless flow field length

Greek symbols

ν_H	fuel stoichiometry
ν_O	oxidant stoichiometry
ρ	water density
φ_O	oxygen fraction in the dry oxidant stream

thermometers completed the array of equipment required to obtain polarization curves, reformate diagnostics, and, temperature, pressure and relative humidity sensitivity curves.

Membrane/electrode assemblies (MEAs) were prepared using proprietary methods. However, some details are given where appropriate to facilitate interpretations (catalyst substrate nature, catalyst loading and location).

3. Results and discussion

3.1. Existence of in-plane gradients in the fuel cell

For illustrative purposes, several gradients (oxygen concentration, temperature, relative humidity) are derived using a common set of assumptions, including: a uniform current distribution, the absence of a net water and reactant fluxes through the MEA, plug flow reactor behavior (uniform concentration at a given location), negligible pressure drop, a dry oxidant inlet, a humidified fuel inlet and ideal gas behavior. Under these conditions, the local gas composition is only modified by the reactant consumption and product accumulation. The first step to calculate the oxygen concentration is to derive an oxygen mass balance (Fig. 1a):

$$N_O(X) - \frac{iA\,dX}{4F} - N_O(X + dX) = 0 \quad (1)$$

Integration of Eq. (1) from $X = 0$ to $X = X$ leads to:

$$N_O(X) = N_O(0) - \frac{iAX}{4F} \quad (2)$$

If the reactant stoichiometry is used to define $N_O(0)$, Eq. (2) is rewritten as

$$N_O(X) = \frac{\nu_O iA}{4F} - \frac{iAX}{4F} \quad (3)$$

The second step consist in deriving a total gas mass balance (oxygen, nitrogen, water vapor, Fig. 1a):

$$N_g(X) - \frac{iA\,dX}{4F} + \frac{iA\,dX}{2F} - N_g(X + dX) = 0 \quad (4)$$

Integration of Eq. (4) from $X = 0$ to $X = X$ leads to:

$$N_g(X) = N_g(0) + \frac{iAX}{4F} \quad (5)$$

If the reactant stoichiometry and oxygen fraction in the dry oxidant stream are used to define $N_g(0)$, Eq. (5) is rewritten as (dry inlet oxidant):

$$N_g(X) = \frac{\nu_O iA}{4\varphi_O F} + \frac{iAX}{4F} \quad (6)$$

In Eq. (6), it was assumed that the gas phase is saturated with water vapor (worst case). The local oxygen concentration is finally obtained by computing the ratio of the oxygen flux to the total gas flux:

$$c_O(X) = \frac{N_O(X)}{N_g(X)} \quad (7)$$

With Eqs. (3) and (6), Eq. (7) reduces to

$$c_O(X) = \frac{(\nu_O iA/4F) - (iAX/4F)}{(\nu_O iA/4\varphi_O F) + (iAX/4F)} = \frac{\nu_O - X}{(\nu_O/\varphi_O) + X} \quad (8)$$

It should be noted that in the best case (low operating temperature), almost all of the water produced is in the liquid phase. In this particular case, the third term on the left hand side of Eq. (4) could be eliminated. The ratio between these extreme oxygen concentration profiles (best and worst cases) could be demonstrated to be $((\nu_0/\varphi_0 + X)/(\nu_0/\varphi_0 - X))$ and has the largest value at $X = 1$ (1.22 for a stoichiometry of 2). Many operating conditions would lead to oxygen concentrations located between these extreme cases. It is assumed here

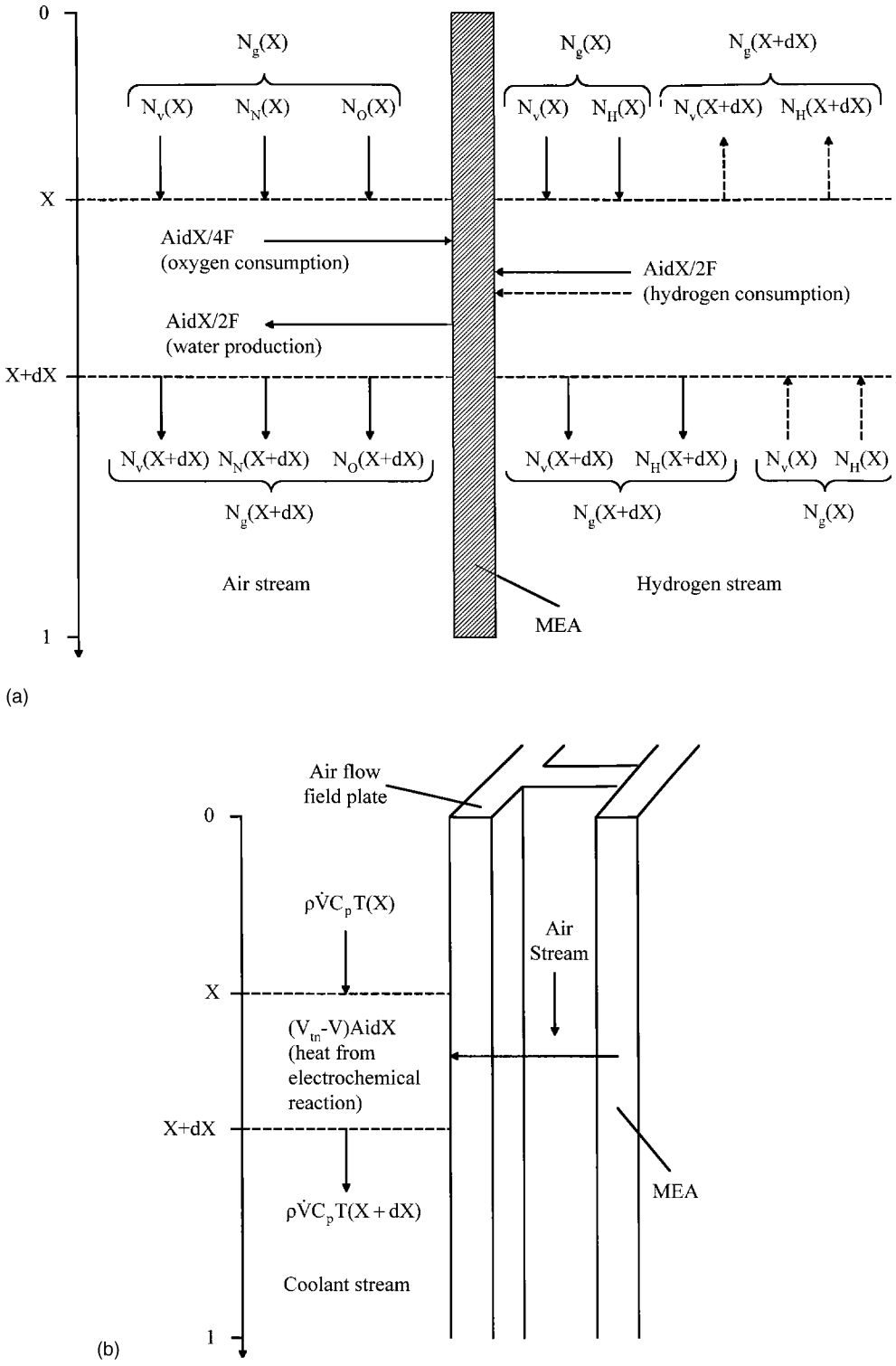

Fig. 1. Schematic representation of the fuel cell, control volumes, mass balance terms (a) and heat balance terms (b). In (a), full lines represent the co-flow configuration case whereas in (b), the dotted lines represent the counter-flow configuration case for the fuel (for the oxidant, the fluxes and their direction are the same irrespective of the flow configuration).

that the error in oxygen concentration implied by Eq. (8) (<22%) is acceptable for demonstration purposes. The dimensionless oxygen concentration (normalized using the oxygen concentration at $X = 0$) is plotted as a function of the dimensionless flow field length for several oxidant stoichiometries in Fig. 2 (parameter values used are given in Table 1). For large stoichiometries, the oxygen concentration change across the flow field length is relatively small and as a

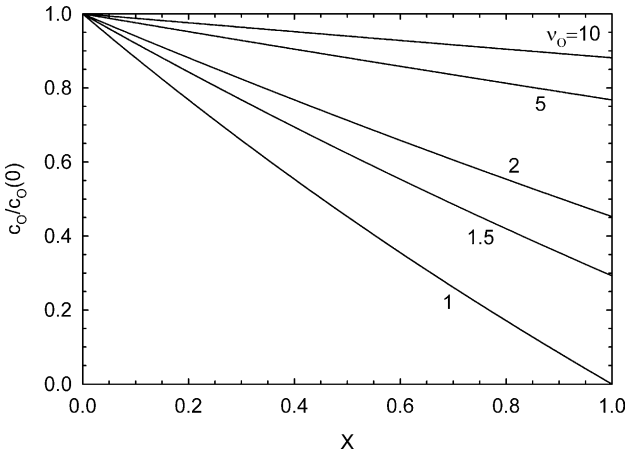

Fig. 2. Dimensionless oxygen concentration profiles across a PEFC serpentine flow field computed using Eq. (8) for different oxidant stoichiometries.

consequence this effect can be ignored. This is the strategy employed by many researchers concerned with aspects of the technology such as catalyst development to simplify data interpretations. However, for low stoichiometries, which are used in practice to reduce parasitic loads associated with gas compression, the oxygen concentration change across the flow field length is significant and cannot be ignored.

Other gradients also exist within a practical fuel cell for similar reasons. For example, the dimensionless temperature distribution is easily obtained for a cell if heat transfer mechanisms to its environment besides coolant forced convection are considered negligible (radiation, conduction to surroundings, natural convection, reactant forced convection) and the voltage distribution is assumed to be fairly uniform [1]. The heat is therefore carried away from the MEA where it is produced ($(V_{tn} - V)iA\,dX$, [16]) through conduction in the flow field plate to the coolant flow field where it is removed by forced convection of the coolant (Fig. 1b). The heat balance is therefore:

$$\rho\dot{V}C_pT(X) + (V_{tn} - V)iA\,dX - \rho\dot{V}C_pT(X + dX) = 0 \quad (9)$$

Integration of Eq. (9) from $X = 0$ to $X = X$ and use of $T(0) = T_0$ leads to:

$$T(X) = T_0 + \frac{iAX(V_{tn} - V)}{\rho\dot{V}C_p} \quad (10)$$

With Eq. (10), the local relative humidity is also determined [1]. The first step is the derivation of the water vapor mass balance (Fig. 1a):

$$N_v(X) + \frac{iA\,dX}{2F} - N_v(X + dX) = 0 \quad (11)$$

Integration of Eq. (11) from $X = 0$ to $X = X$ leads to (remembering the dry oxidant inlet assumption):

$$N_v(X) = \frac{iAX}{2F} \quad (12)$$

The fraction of water vapor in the gas stream at any location is obtained by computing the ratio of the water vapor flux (Eq. (12)) to the total gas flux (Eq. (6)). Multiplying the water vapor fraction in the gas stream by the total gas pressure leads to the water vapor partial pressure (ideal gas behavior) which can be combined with the relative humidity definition:

$$RH(X) = \frac{p_v(X)}{p_s(X)} = \frac{pN_v(X)}{p_s(X)N_g(X)} \quad (13)$$

An explicit expression of the relative humidity is obtained by introducing Eqs. (6) and (12) into Eq. (13):

$$RH(X) = \frac{p(iAX/2F)}{p_s(X)((\nu_O iA/4\varphi_O F) + (iAX/4F))} = \frac{2pX}{p_s(X)(\nu_O/\varphi_O + X)} \quad (14)$$

The water vapor saturation pressure term appearing in Eq. (14) is obtained from the empirical Eq. (15) [1] in combination with Eq. (10).

$$\log p_s(X) = -2.1794 + 0.02953T(X) - 9.1837 \times 10^{-5}T(X)^2 + 1.4454 \times 10^{-7}T(X)^3 \quad (15)$$

It should be noted that relative humidity values >100% indicate the presence of liquid water in the reactant stream. Fig. 3 shows the gradients computed by Eqs. (8), (10) and (14) for oxygen concentration, oxidant relative humidity, fuel relative humidity and temperature (in this case, the gradient is normalized using the temperature at $X = 0$).

Table 1
List of the parameter values used to compute curves appearing in Figs. 2 and 3

Parameter	Value
A (cm^2)	300
C_p (J/(g °C))	4.2
i (A/cm^2)	1
p (atm)	3.04
$p_{s,0}$ (atm at 75 °C)	0.380
$p_{s,1}$ (atm at 86.8 °C)	0.612
RH_0 (co-flow)	0.805
RH_1 (counter-flow)	0.5
T_0 (°C)	75
V (V)	0.6
V_{tn} (V)	1.562
$\dot{V}$ (cm^3/s)	6
ν_H	1.5
ν_O	1–10
φ_O	0.21
ρ (g/cm^3)	0.97

3.2. Manipulation of in-plane gradients in the fuel cell for higher performance

In order to achieve peak performance in the fuel cell, it is important that all the gradients are properly matched. Manipulation of in-plane gradients can be designed to

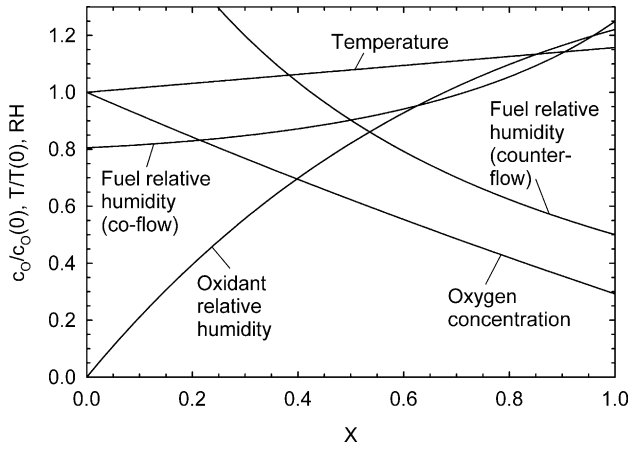

Fig. 3. Dimensionless oxygen concentration and temperature profiles, and relative humidity profiles across a PEFC serpentine flow field computed using Eqs. (8), (10), (14), (18), and (25).

minimize all performance loss types (ohmic, mass transport, kinetic, reformate). For example, near the cell outlet, the oxygen concentration is low (Fig. 2) which leads to more pronounced mass transfer issues. This situation is worsened by product water accumulation (some liquid water is present, Fig. 2). It is important to develop in-plane gradients that can reduce these mass transport issues and the associated liquid water accumulation.

Effective water management has a major impact on fuel cell performance. Peak fuel cell power is achieved typically at higher current densities where performance can be limited by mass transport issues usually associated with water management. A number of water management strategies have been considered by Ballard [1,17] and others but perhaps the most easy and reliable methods to implement are those based on flow field design and operating conditions. A pressure drop gradient and/or temperature rise gradient between the inlet and outlet of the flow field can be used to increase the water vapor carrying capacity of the gas [18,19].

The effectiveness of a temperature rise gradient is shown in Fig. 4. The cell performance is plotted as a function of the temperature difference between the coolant inlet and outlet. As the temperature difference increases, the air performance also increases because the oxidant stream can store more water in the vapor form thus decreasing mass transfer issues near the cell outlet. The decrease in mass transfer issues is also demonstrated by the performance difference obtained with air and helox (a 79/21% helium/oxygen mixture facilitating oxygen mass transfer). The performance difference between these two oxidants decreases with the increase in the temperature difference between inlet and outlet indicating a reduction in oxygen mass transfer issues. However, care needs to be exercised when using this strategy to avoid dehydrating the membrane. With larger temperature differences, the membrane resistance increases, which will reduce cell performance.

The pressure drop gradient strategy is similar to the temperature rise gradient since in both cases the underlying assumption is to match the amount of water the gas stream can carry with excess water being produced. The results obtained with the pressure drop strategy are also essentially the same in character. As observed in Fig. 5, an increase in cell performance is first observed, attributed to a decrease in liquid water related mass transfer issues. At larger pressure drop values, the cell performance suffers because water removal is enhanced to such an extent that membrane dehydration occurs.

The use of pressure drop or increased gas flow velocity to evaporate liquid water and/or assist liquid water to become entrained into the gas stream usually has an associated system parasitic load. The energy required for gas delivery is directly related to pressure, volume flow rate and pressure drop. For temperature rise, the coolant flow rate is regulated which generally results in less of a system parasitic load. In

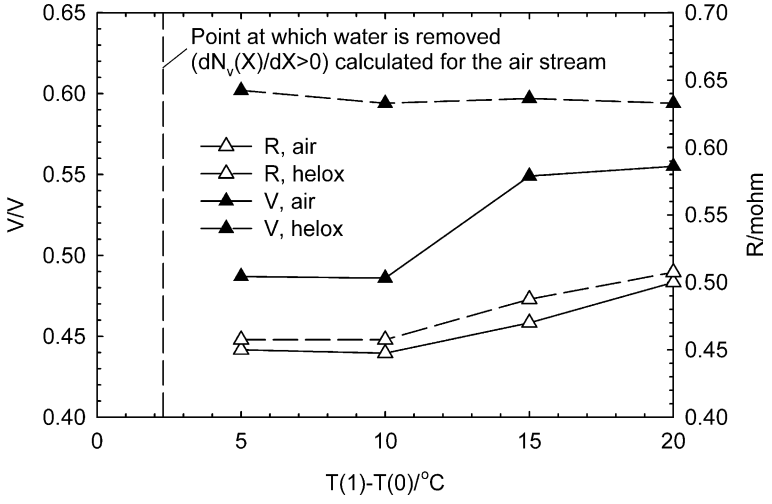

Fig. 4. Average cell voltage and resistance (four MEAs) as a function of the temperature rise across a PEFC serpentine flow field for different oxidants. Inlet conditions: oxidant/H_2, 2/1.5 stoichiometry, 80% relative humidity, 3.08 bar abs, 75 °C (70 °C for $T(1) - T(0) = 20$ °C), 1.08 A/cm^2.

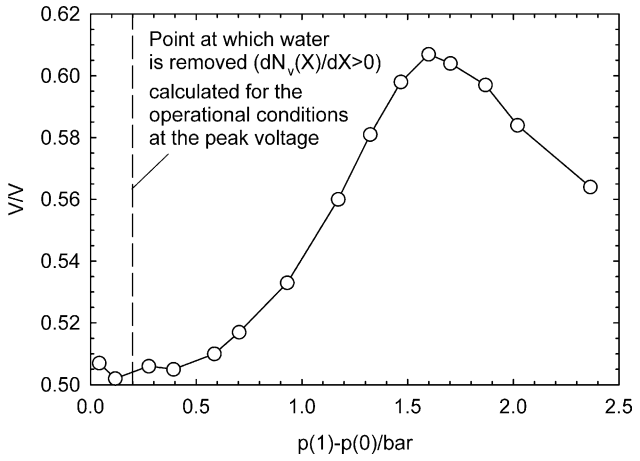

Fig. 5. Cell voltage as a function of the pressure drop across a PEFC serpentine flow field. Inlet conditions: air/H_2, 2/1.18–26.27 stoichiometry, 100% relative humidity, 4.46 bar abs, 70 °C, 1.29 A/cm^2.

practice, the best performance results are usually achieved with a combination of pressure drop and temperature rise.

Flow field water management approaches in conjunction with appropriate in-plane gradients can allow fuel cell operation with reduced to zero humidification [20]. This approach is best illustrated by computing the fuel relative humidity for two cases (fuel is directed either in co- or counter-flow with respect to both the oxidant and coolant streams, Fig. 1a). The relative humidity for the co-flow case is obtained in a similar manner as for the oxidant stream previously discussed. The equivalent water vapor and total gas (water vapor, hydrogen) mass balances, and relative humidity equations are (wet fuel inlet):

$$N_v(X) = N_v(0) = N_{v,0} \tag{16}$$

$$N_g(X) = N_{v,0} + \frac{v_H iA}{2F} - \frac{iAX}{2F} \tag{17}$$

$$\mathrm{RH}(X) = \frac{pN_v(X)}{p_s(X)N_g(X)} = \frac{pN_{v,0}}{p_s(X)(N_{v,0} + (v_H iA/2F) - (iAX/2F))} \tag{18}$$

Eq. (18) with $X = 0$, $\mathrm{RH}(0) = \mathrm{RH}_0$, $p_s(0) = p_{s,0}$ and isolating $N_{v,0}$ reduces to:

$$N_{v,0} = \frac{\mathrm{RH}_0 p_{s,0}(v_H iA/2F)}{p - \mathrm{RH}_0 p_{s,0}} \tag{19}$$

The relative humidity for the counter-flow case is obtained by first deriving the water vapor mass balance (Fig. 1a):

$$-N_v(X) + N_v(X + \mathrm{d}X) = 0 \tag{20}$$

Integration of Eq. (20) from $X = 1$ to $X = X$ leads to:

$$N_v(X) = N_v(1) = N_{v,1} \tag{21}$$

For the counter-flow case, the total gas mass balance is

$$-N_g(X) - \frac{iA\,\mathrm{d}X}{2F} + N_g(X + \mathrm{d}X) = 0 \tag{22}$$

Integration of Eq. (22) from $X = 1$ to $X = X$ leads to:

$$N_g(X) = N_g(1) + \frac{iA}{2F}(X - 1) \tag{23}$$

If the reactant stoichiometry is used to define $N_g(1)$ and care is taken to include the water vapor flux, Eq. (23) is rewritten as

$$N_g(X) = N_{v,1} + \frac{v_H iA}{2F} + \frac{iA}{2F}(X - 1) \tag{24}$$

An explicit expression of the relative humidity is obtained by introducing Eqs. (21) and (24) into Eq. (13):

$$\mathrm{RH}(X) = \frac{pN_v(X)}{p_s(X)N_g(X)} = \frac{pN_{v,1}}{p_s(X)(N_{v,1} + (v_H iA/2F) + (iA/2F)(X - 1))} \tag{25}$$

Eq. (25) with $X = 1$, $\mathrm{RH}(1) = \mathrm{RH}_1$, $p_s(1) = p_{s,1}$ and isolating $N_{v,1}$ reduces to:

$$N_{v,1} = \frac{\mathrm{RH}_1 p_{s,1}(v_H iA/2F)}{p - \mathrm{RH}_1 p_{s,1}} \tag{26}$$

The profiles obtained from Eqs. (18) and (25) using the same amount of water vapor introduced in the cell (Eqs. (19) and (26) are useful to compute the respective relative humidities for $N_{v,0} = N_{v,1}$) are illustrated in Fig. 3. In the co-flow case, the fuel relative humidity profile is not properly matched to the oxidant profile because the oxidant inlet is relatively dry (both the fuel and oxidant relative humidity are less than 100%). However, for the counter-flow case, a better gradient match is achieved because the oxidant inlet is not so dry (the fuel stream contains some liquid water which can partly diffuse through the membrane towards the oxidant compartment) and the oxidant outlet benefits from a relatively dry fuel inlet, which relieves water related mass transfer issues. Therefore, the counter-flow case offers the prospect of better performance when low gas relative humidities are used. This is confirmed by data illustrated in Fig. 6. In both cases, the cell performance increases with the decrease in inlet oxidant relative humidity, which is attributable to less liquid water mass transfer issues. However, the cell performance increase is smaller for the co-flow case because the membrane dehydration at the cell inlet is more severe, as revealed by the resistance measurements, due to the relative dryness of the oxidant inlet area.

Another method to increase cell performance is to modify the MEA in-plane to ensure that its properties match the gradient of interest. In-plane modification of the electrode substrate to form a non-uniform structure can be used to control reactant and product transport [21]. For example, as discussed previously liquid water management issues are especially acute near the cell outlet region (Fig. 3). It is possible to modify the gas diffusion electrode in such a way as to locally enhance both oxygen and water transport by

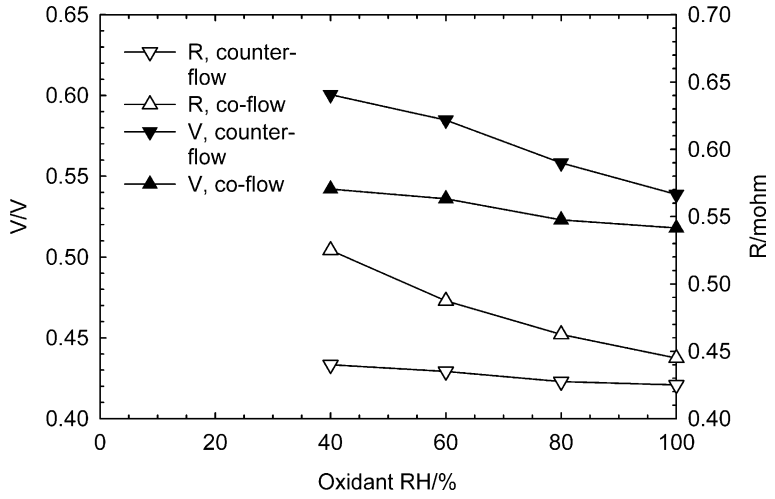

Fig. 6. Average cell voltage and resistance (four MEAs) as a function of the inlet oxidant relative humidity for different gas flow field configurations. Inlet conditions: air/H_2, 2/1.5 stoichiometry, 80% fuel relative humidity, 3.08 bar abs, 80 °C (90 °C outlet), 1.08 A/cm^2.

increasing porosity. For example, this can be achieved by creating grooves or holes in the substrate or by using a different more porous substrate than the commonly used carbon fiber paper (such as carbon cloth). Fig. 7 shows the results obtained with such non-uniform MEA structures. In each case and at large current densities where water management issues are more prominent, cell performance was improved with respect to a baseline MEA not subject to any modification. Some voltage losses are also observed at low current densities, where kinetic losses predominate, in some cases and are attributed to a decreased catalyst area (pierced and carbon cloth substrates).

In-plane gradients in catalyst distribution can be used to enhance performance and enhance the efficient use of platinum group metals [22]. For example, it is possible to increase cell performance by redistributing the cathode catalyst near the oxidant inlet where the larger oxygen concentration could reduce kinetic losses (the oxygen reduction reaction is first order with respect to oxygen concentration). This approach was investigated by grading the MEA catalyst loading from the oxidant inlet to the outlet using three separate sections and a 4/2/1 ratio between their respective catalyst loading. The results are illustrated in Fig. 8, and confirm the kinetic gain hypothesis at low current densities. However, this approach has an additional benefit related to mass transfer losses. The use of this strategy modifies the current distribution so that a larger proportion of the current is located near the oxidant inlet. As a consequence, the region where liquid water mass transfer issues normally arise (in absence of a catalyst distribution gradient) is more extended (lower localized current density), therefore, enhancing oxygen mass transfer rates and reducing mass transfer related performance losses at large current densities. It should be noted that if only a kinetic gain was

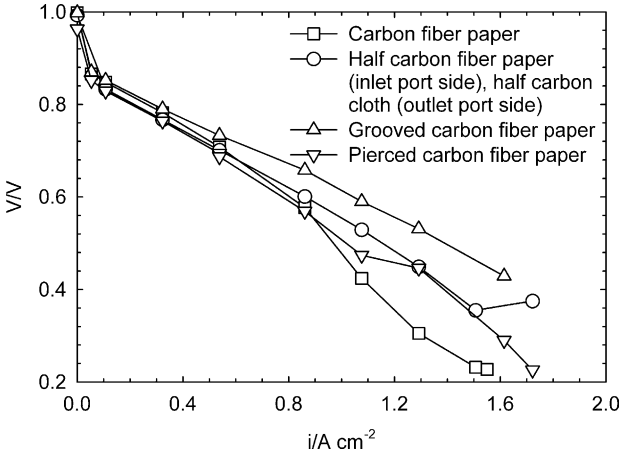

Fig. 7. Polarization curves obtained with different cathode gas diffusion layer modifications to reduce mass transport losses. Inlet conditions: air/H_2, 2/1.5 stoichiometry, 100% relative humidity, 3.08 bar abs, 80 °C.

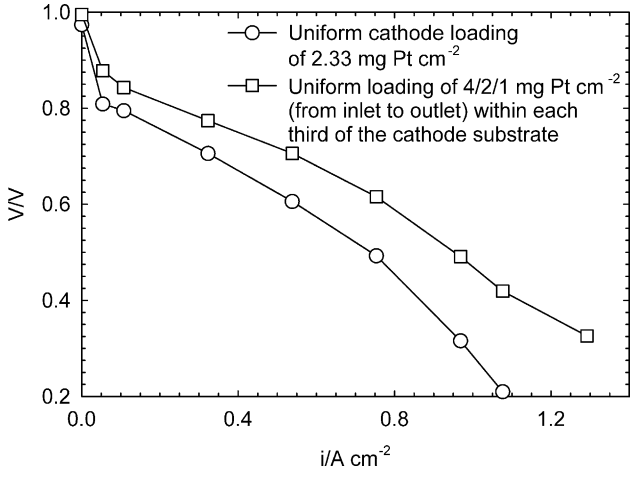

Fig. 8. Polarization curves obtained with different cathode catalyst distributions to reduce kinetic losses. Inlet conditions: air/H_2, 2/1.5 stoichiometry, 100% relative humidity, 3.08 bar abs, 80 °C.

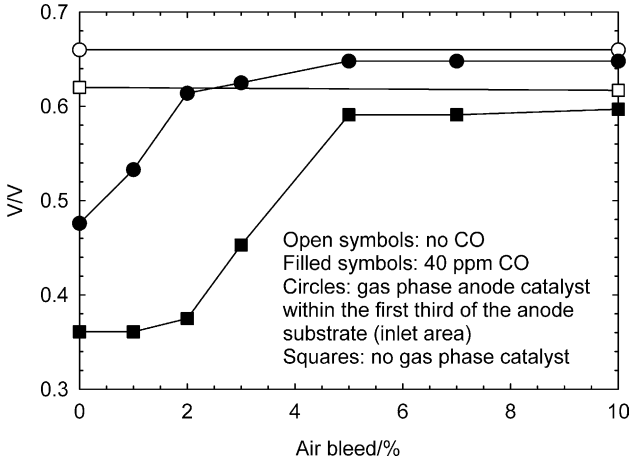

Fig. 9. Air bleed sensitivity curves obtained with different gas phase CO oxidation catalyst distributions. Inlet conditions: air/simulated reformate (70/30% H_2/N_2 with and without CO), 2/1.5 stoichiometry, 100% relative humidity, 3.08 bar abs, 80 °C, 0.75 A/cm^2.

observed, the voltage difference between the two polarization curves would be constant and would not increase at high current densities.

For the anode, in-plane gradients or non-uniformities in catalyst distribution can also be used to enhance the efficient use of platinum group metals. For example, the presence of a gas phase catalyst region in the anode promotes the more efficient oxidation of the carbon monoxide (reformate fuel) with air injection before it reaches the electrocatalyst containing layer [22,23]:

$$2CO + O_2 \rightarrow 2CO_2 \quad (27)$$

This gas phase catalyst layer is conventionally applied as a uniform layer over the entire active area to oxidize trace amounts of carbon monoxide which poison the electrocatalyst and reduce fuel cell performance. However, it is possible to achieve similar results with less gas phase catalyst by localizing the catalyst near the fuel inlet to ensure that the greatest reduction in carbon monoxide concentration is achieved in this region when an air bleed is introduced. The results obtained with such a beneficial strategy and a simulated reformate are illustrated in Fig. 9. The carbon monoxide air bleed sensitivity is significantly improved at a low percentage air bleed.

4. Conclusion

Manipulation of in-plane gradients in the fuel cell has been shown to improve performance. Beneficial gradients can be formed by manipulating operating conditions over the active area of the fuel cell and by use of non-uniform MEA structures. In addition to the approaches discussed here, other methods can be developed to manage gradients within fuel cells. For example, a distributed reactant feed and gas enrichment strategies can be used to modify the reactant concentration gradient which could beneficially impact kinetic and mass transport performance losses [24–27]. Manufacturing plays an important role in fuel cell cost reduction strategies, which would be supported by the adoption of simple, uniform stack designs. From this point of view, methods aimed at modifying operating conditions (temperature rise, pressure drop, flow configuration) are preferable than non-uniform MEA structures (gas diffusion electrode, electrocatalyst and gas phase catalyst distribution).

References

[1] J. St-Pierre, D.P. Wilkinson, H. Voss, R. Pow, in: O. Savadogo, P.R. Roberge (Eds.), Proceedings of the 2nd International Symposium on New Materials for Fuel Cell and Modern Battery Systems, École Polytechnique, Montréal, 1997, p. 318.
[2] A.C. West, T.F. Fuller, J. Appl. Electrochem. 26 (1996) 557.
[3] J.H. Lee, T.R. Lalk, A.J. Appleby, J. Power Sources 70 (1998) 258.
[4] G. Maggio, V. Recupero, C. Mantegazza, J. Power Sources 62 (1996) 167.
[5] F. Standaert, K. Hemmes, N. Woudstra, J. Power Sources 63 (1996) 221.
[6] F. Standaert, K. Hemmes, N. Woudstra, J. Power Sources 70 (1998) 181.
[7] T.F. Fuller, J. Newman, J. Electrochem. Soc. 140 (1993) 1218.
[8] T.V. Nguyen, R.E. White, J. Electrochem. Soc. 140 (1993) 2178.
[9] H.P.L.H. van Bussel, F.G.H. Koene, R.K.A.M. Mallant, J. Power Sources 71 (1998) 218.
[10] J.S. Yi, T.V. Nguyen, J. Electrochem. Soc. 145 (1998) 1149.
[11] P.C. Rieke, N.E. Vanderborgh, J. Electrochem. Soc. 134 (1987) 1099.
[12] S.J.C. Cleghorn, C.R. Derouin, M.S. Wilson, S. Gottesfeld, J. Appl. Electrochem. 28 (1998) 663.
[13] J. Stumper, S.A. Campbell, D.P. Wilkinson, M.C. Johnson, M. Davis, Electrochim. Acta 43 (1998) 3773.
[14] J.J.T.T. Vermeijlen, L.J.J. Janssen, A.J. Geurts, G.C. van Haastrecht, J. Appl. Electrochem. 25 (1995) 1122.
[15] A. Neubrand, J. Appl. Electrochem. 28 (1998) 1179.
[16] K. Scott, Electrochemical Reaction Engineering, Academic Press, London, 1991, p. 463.
[17] H.H. Voss, D.P. Wilkinson, P.G. Pickup, M.C. Johnson, V. Basura, Electrochim. Acta 40 (1995) 321.
[18] H.H. Voss, D.P. Wilkinson, D.S. Watkins, US Patent No. 5 260 143 (9 November 1993); US Patent No. 5 441 819 (15 August 1995).
[19] N.J. Fletcher, C.Y. Chow, E.G. Pow, B.M. Wozniczka, H.H. Voss, G. Hornburg, D.P. Wilkinson, US Patent No. 5 547 776 (20 August 1996).
[20] D.P. Wilkinson, H.H. Voss, N.J. Fletcher, M.C. Johnson, E.G. Pow, US Patent No. 5 773 160 (30 June 1998).
[21] M.C. Johnson, D.P. Wilkinson, C.P. Asman, M.L. Bos, R.J. Potter, US Patent No. 5 840 438 (24 November 1998).
[22] J.C. Frost, J.M. Gascoyne, G.A. Hards, D.P. Wilkinson, K.B. Prater, US Patent No. 5 702 839 (30 December 1997).
[23] D.P. Wilkinson, H.H. Voss, K.B. Prater, G.A. Hards, T.R. Ralph, D. Thompsett, US Patent No. 5 795 669 (18 August 1998).
[24] J. St-Pierre, N. Jia, J. New Mater. Electrochem. Syst. 5 (2002).
[25] D.P. Wilkinson, J. St-Pierre, in: W. Vielstich, H. Gasteiger, A. Lamm (Eds.), Handbook of Fuel Cells—Fundamentals, Technology and Applications, vol. 3, Wiley, New York, 2003 (Chapter 53).
[26] D.P. Wilkinson, H.H. Voss, J. Dudley, G.J. Lamont, V. Basura, US Patent No. 5 482 680 (9 January 1996).
[27] D.P. Wilkinson, H.H. Voss, J. Dudley, G.J. Lamont, V. Basura, US Patent No. 5 432 021 (11 July 1995).